Controlled Electrochemical Intercalation of Graphene/*h*-BN van der Waals Heterostructures

S. Y. Frank Zhao,[†] Giselle A. Elbaz,[‡] D. Kwabena Bediako,[†] Cyndia Yu,[†] Dmitri K. Efetov,[§] Yinsheng Guo,[‡] Jayakanth Ravichandran,[†] Kyung-Ah Min,[∥] Suklyun Hong,[∥] Takashi Taniguchi,[⊥] Kenji Watanabe,[⊥] Louis E. Brus,[‡] Xavier Roy,[‡] and Philip Kim*,[†]

[†]Department of Physics, Harvard University, Cambridge, Massachusetts 02138, United States
[‡]Department of Chemistry, Columbia University, New York, New York 10027, United States
[§]Department of Physics, Columbia University, New York, New York 10027, United States
[∥]Department of Physics and Graphene Research Institute, Sejong University, Seoul 143-747, South Korea
[⊥]National Institute for Materials Science, 1-1 Namiki, Tsukuba, Ibaraki 305-0044, Japan

S Supporting Information
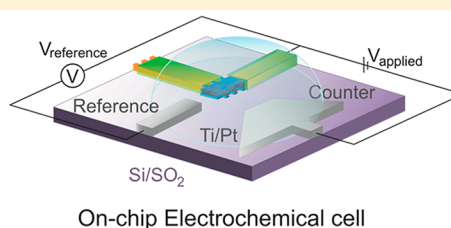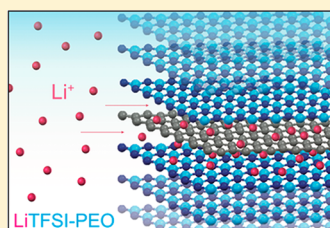
ABSTRACT: Electrochemical intercalation is a powerful method for tuning the electronic properties of layered solids. In this work, we report an electrochemical strategy to controllably intercalate lithium ions into a series of van der Waals (vdW) heterostructures built by sandwiching graphene between hexagonal boron nitride (*h*-BN). We demonstrate that encapsulating graphene with *h*-BN eliminates parasitic surface side reactions while simultaneously creating a new heterointerface that permits intercalation between the atomically thin layers. To monitor the electrochemical process, we employ the Hall effect to precisely monitor the intercalation reaction. We also simultaneously probe the spectroscopic and electrical transport properties of the resulting intercalation compounds at different stages of intercalation. We achieve the highest carrier density $>5 \times 10^{13}$ cm^2 with mobility $>10^3$ cm^2/(V s) in the most heavily intercalated samples, where Shubnikov−de Haas quantum oscillations are observed at low temperatures. These results set the stage for further studies that employ intercalation in modifying properties of vdW heterostructures.

KEYWORDS: *Nanoscale electrochemistry, graphite intercalation, graphene, van der Waals heterostructures, host−guest*

Graphite intercalation compounds (GICs) exhibit a variety of interesting properties that differ significantly from semimetal graphite.[1] For example, CaC$_6$ and YbC$_6$ display superconductivity,[2] while Li$_{0.25}$Eu$_{1.95}$C$_6$ and EuC$_6$ exhibit ferro- and antiferromagnetic ordering, respectively.[3] Intercalation compounds also represent technologically significant materials. LiC$_6$ is the prototypical anode material in Li ion batteries. By analogy to these bulk graphite intercalation compounds, the intercalation of few-layer graphene has also been realized.[4−6] Upon intercalation of Li, the optical properties of few-layer graphene crystals (with thicknesses down to 1 nm) change significantly,[4] Ca-intercalated few-layer-graphene is super-conducting,[5] and FeCl$_3$ intercalated bilayer graphene showed a hint of ferromagnetism.[6] In addition, there have been theoretical predictions that heavy doping and proximity induced spin−orbit coupling from certain intercalants may induce exotic electronic properties in the graphene channel.[7]

Recently, it was demonstrated that one can stack different van der Waals (vdW) atomic layers to form vdW heterostructures, creating a new generation of few-atomic-layer functional heterostructures with emergent properties.[8,9] In particular, graphene encapsulated by *h*-BN, a layered insulator, forms a vdW heterostructure where the two-dimensional (2D) graphene channel is well isolated from the environment.[8] As in intercalation compounds of bulk vdW materials, the intercalation of vdW heterostructures may create a new generation of functional heterostructures with emergent properties. Furthermore, the use of *h*-BN protecting layers may enable the formation of stable intercalation compounds that differ significantly from the bulk intercalation compound due
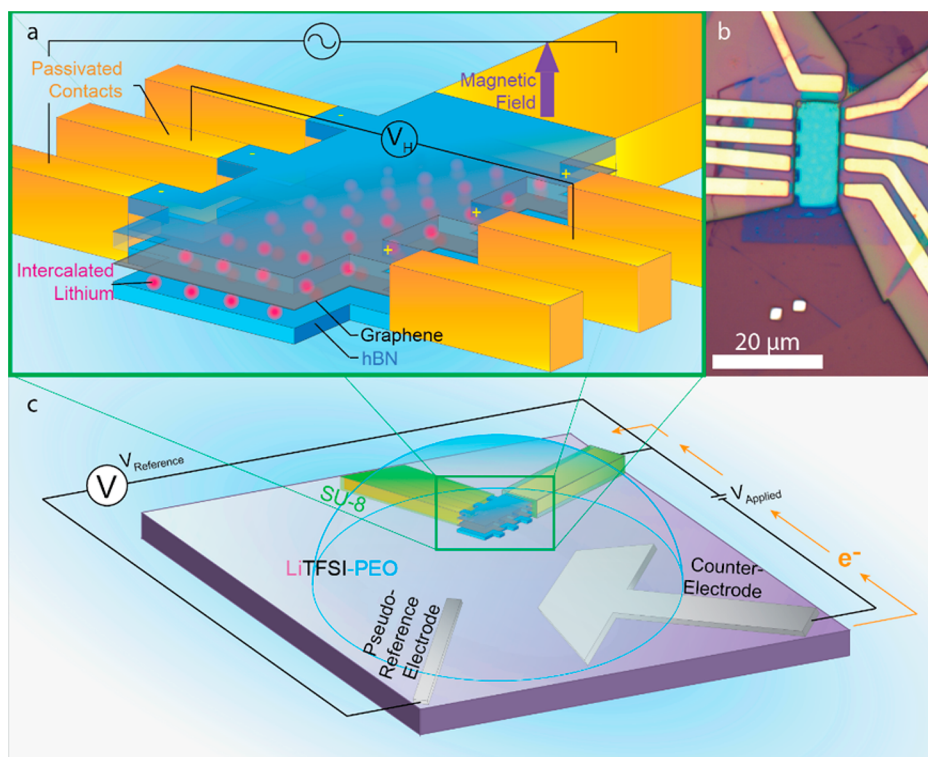
Figure 1. (a) Schematic of the Hall bar device. A *h*-BN/graphene/*h*-BN heterostructure is patterned into a Hall bar with edge Cr/Pd/Au (2/15/60 nm) contacts. A channel is left open at the entrance of the Hall bar to allow interactions with the electrolyte. An AC current is applied across the device in a 0.5 T magnetic field, inducing a transverse Hall voltage across the device. The Hall voltage is used to monitor the intercalation reaction. (b) Optical micrograph of a representative heterostructure device before electrolyte deposition. Note that all electrodes are covered with SU-8 photoresist, leaving only an edge of graphene in contact with the electrolyte. (c) The solid polymer LiTFSI−PEO electrolyte is dropcast over the Hall bar device (working electrode) shown in part a as well as a Pt pseudoreference electrode and counter electrode. To drive the electrochemical reaction, a voltage is applied between the counter electrode and working electrode, and the intercalation voltage is measured versus a Pt pseudoreference.

to the presence of two dissimilar surfaces at the heterointerface.[10]

Compared to traditional intercalation methods for van der Waals materials, these synthetic *h*-BN/graphene vdW heterostructures present several challenges for intercalation. For example, bulk alkali metal intercalated vdW crystals are chemically highly unstable, prohibiting subsequent exfoliation into few-atomic-layer intercalated nanocrystals. Conversely, conventional chemical intercalation methods involve highly reactive reagents and high temperatures,[1] often incompatible with microfabrication procedures for electronic device characterization. Another challenge associated with electrochemical intercalation of atomically thin vdW heterostructures stems from the difficulties in measuring the sub-picoampere electrochemical currents produced from atomically thin van der Waals structures having micron-size lateral dimensions. Such a small current can easily be dominated by current contributions from parasitic reactions occurring in the electrolyte, precluding the use of standard electrochemistry techniques such as cyclic voltammetry.

Our strategy to overcome these hurdles was to employ an electrochemical technique on a prefabricated mesoscopic electrical device, thus replacing conventional molten metal reagents with a relatively inert electrolyte, and using the applied bias to deliver a controllable driving force. We demonstrate (i) that *h*-BN is an effective passivation layer for 2D devices with respect to electrochemical degradation; (ii) the formation of a prototype heterostructure intercalation

compound and show for the first time the insertion of Li ions into the interface between single-layer graphene and *h*-BN crystals; and (iii) the use of the Hall effect to monitor the progress of intercalation as a function of applied bias, rather than standard voltammetry methods.[11] Our approach is not restricted only to graphene/*h*-BN heterostructures, or only to the intercalation of Li; it can be generalized to a wide range of heterostructures, opening the field to a new system of intercalation compounds.

In our experiment, we use mechanical exfoliation followed by van der Waals dry assembly techniques[12] to fabricate vdW heterostructures, using monolayer (1LG) or bilayer (2LG) graphene sandwiched between ∼30 nm thick *h*-BN crystals. The vdW stacks are then shaped into Hall bar geometries, with only the well-defined graphene edges in the vdW stack exposed to the electrolyte. Intercalation is thus only allowed from the edge of the sample (Figure 1b). Using this technique, we can unambiguously and directly observe the reversible doping of graphene as Li ions intercalate and de-intercalate the *h*-BN/graphene interface, despite any side reactions that take place at electrolyte-exposed conducting surfaces. Figure 1 depicts the basic design of our electrochemical cell. Here, we use the graphene channel as a working electrode. The graphene channel itself is electrically contacted by gold electrodes using the edge contact method.[12] All gold contacts and wires in our devices are covered with a passivating SU-8 layer that is both electrochemically inert and electrically insulating. This simultaneously protects the Au from corrosive reactions
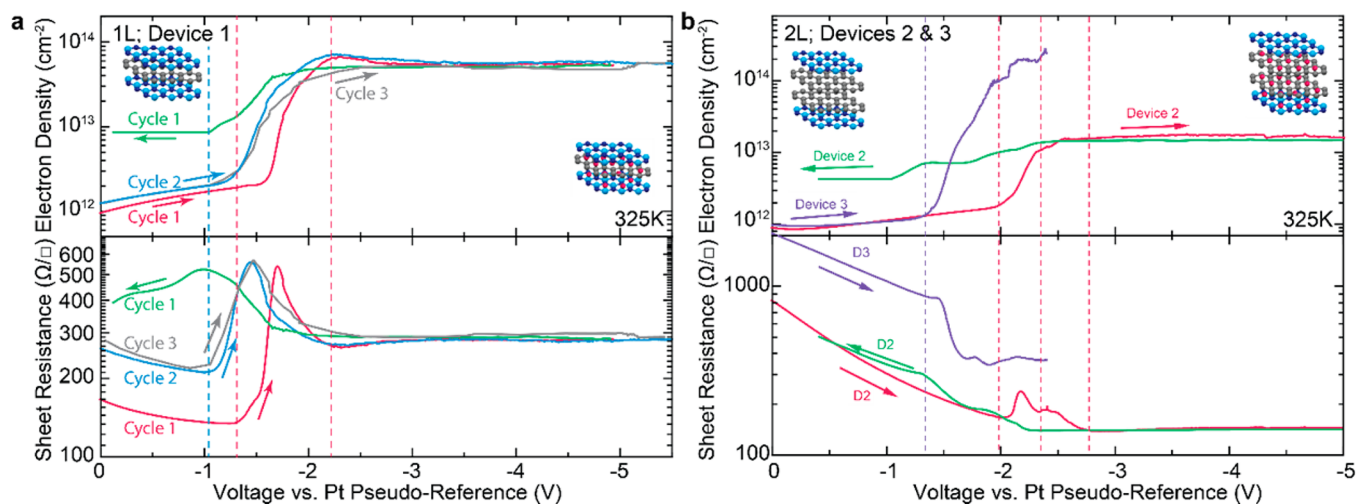
Figure 2. Measured electron density and sample resistivity in intercalating and de-intercalating graphene heterostructures fabricated with (a) one-layer graphene and (b) two-layer graphene. In both cases, on the first intercalation cycle (red), electron density increases linearly at low potentials, while resistance decreases, consistent with electrostatic gating across the h-BN. Once the electrochemical potential exceeds a certain threshold, electron density suddenly increases by about an order of magnitude and then saturates, while at the same time resistance spikes. This suggests the onset of the electrochemical reaction. When the potential is swept back toward zero (green), the sample de-intercalates at a slightly lower voltage but follows the same general trend in reverse. In part a, blue and silver traces show subsequent intercalation cycles on the same device, where the same trend is observed but with a lower threshold voltage. In part b, for the 2LG case, data from a second device is shown instead (purple), showing an intercalation run to the highest achieved electron density in 2LG. This sample is intercalated in an optical cryostat sealed directly inside an argon glovebox, minimizing contamination relative to the other samples sealed in a DIP-16 package using a dried glass coverslip. For details on sample sealing and sample mounting, as well as sweep rates, please see the Supporting Information.

occurring at high voltage and limits the number of side reactions occurring in the cell. The device includes a Pt counter electrode and a Pt pseudoreference electrode. We cover the whole device with a solid electrolyte composed of lithium bis(trifluoromethane)sulfonimide (LiTFSI) suspended in a poly(ethylene oxide) (PEO) matrix. (See detailed methods in the Supporting Information.)

To control the intercalation progress, we monitor intercalation in real time using Hall effect measurements (with a small applied magnetic field of 0.5 T), simultaneously probing the electrical transport properties and the charge carrier density of the crystals as Li ions are inserted.[11] Using this technique, we can unambiguously observe the reversible doping of graphene as Li ions intercalate and de-intercalate the h-BN/graphene interface. Figure 1b shows an optical microscope image of a typical device used for the experiment. To facilitate magneto-transport measurements, the graphene heterostructure is patterned into a Hall bar geometry. Note that the standard Hall bar geometry is modified slightly, with the source contact at the end of the Hall bar split into two on the far side of the device, so that the corresponding etched edge can be exposed directly to the electrolyte.

Figure 2 shows the resistivity and estimated carrier density obtained from Hall measurement for two devices built from 1LG and 2LG sandwiched between h-BN. In both cases, while the electrode potential is swept toward increasingly negative values at 325 K (i.e., toward more reducing potential), the graphene channel carrier density increases linearly with the applied voltage, while the resistance of the sample decreases, consistent with electrostatic gating of the graphene crystal, through the h-BN dielectric, close to the high-resistance Dirac point.[13] As we reach a threshold voltage (~ -1.4 V for cycle 1 in Figure 2a), the carrier density begins to increase at a significantly higher rate, suggesting the intercalation of Li ions into the heterostructure. At the same threshold voltage, we

observe a spike in the sheet resistance of the device, consistent with a decrease in the graphene mobility as charged Li ions move into the device.

The exact threshold voltage value varies somewhat from device to device, where contact resistances between the gold contacts and graphene and between graphene and electrolyte change due to microscopic differences between devices. This results in an ohmic voltage loss between our heterostructure working electrodes and the Pt pseudoreference. With these sample-to-sample variations, the typical threshold voltage is between -1 and -3 V.

On the reverse scan, we observe a concordant steep decrease of the charge carrier density associated with a slightly broader maximum in the resistance of the device. We note that de-intercalation happens at a lower voltage than the initial intercalation threshold voltage. Immediately after de-intercalation, our measurements indicate the graphene heterostructures contain more electrons than the pristine device, suggesting that some Li ions remain between the sheets initially. After holding the device at 0 V overnight (>12 h), the device returns to its fully de-intercalated state where the residual charge density becomes $\sim 10^{12}$ cm^{-2}. Subsequently, a second intercalation sweep in the same geometry reveals a response very similar to the first intercalation. Overall, the reversibility of the reaction demonstrates that our measurements are not a result of a sudden delamination of the van der Waals heterostructure, which would result in a permanent increase of electrostatic gating efficiency at all potentials.

These Hall potentiometry data demonstrate that the reversible electrochemical intercalation and de-intercalation of Li ions in the interface between graphene and h-BN crystals is possible. For 2LG samples, the intercalated Li ions can insert either in the graphene/graphene interface or in the graphene/h-BN interfaces. Raman spectroscopy is a useful probe to investigate the distribution of intercalation in few-layer-
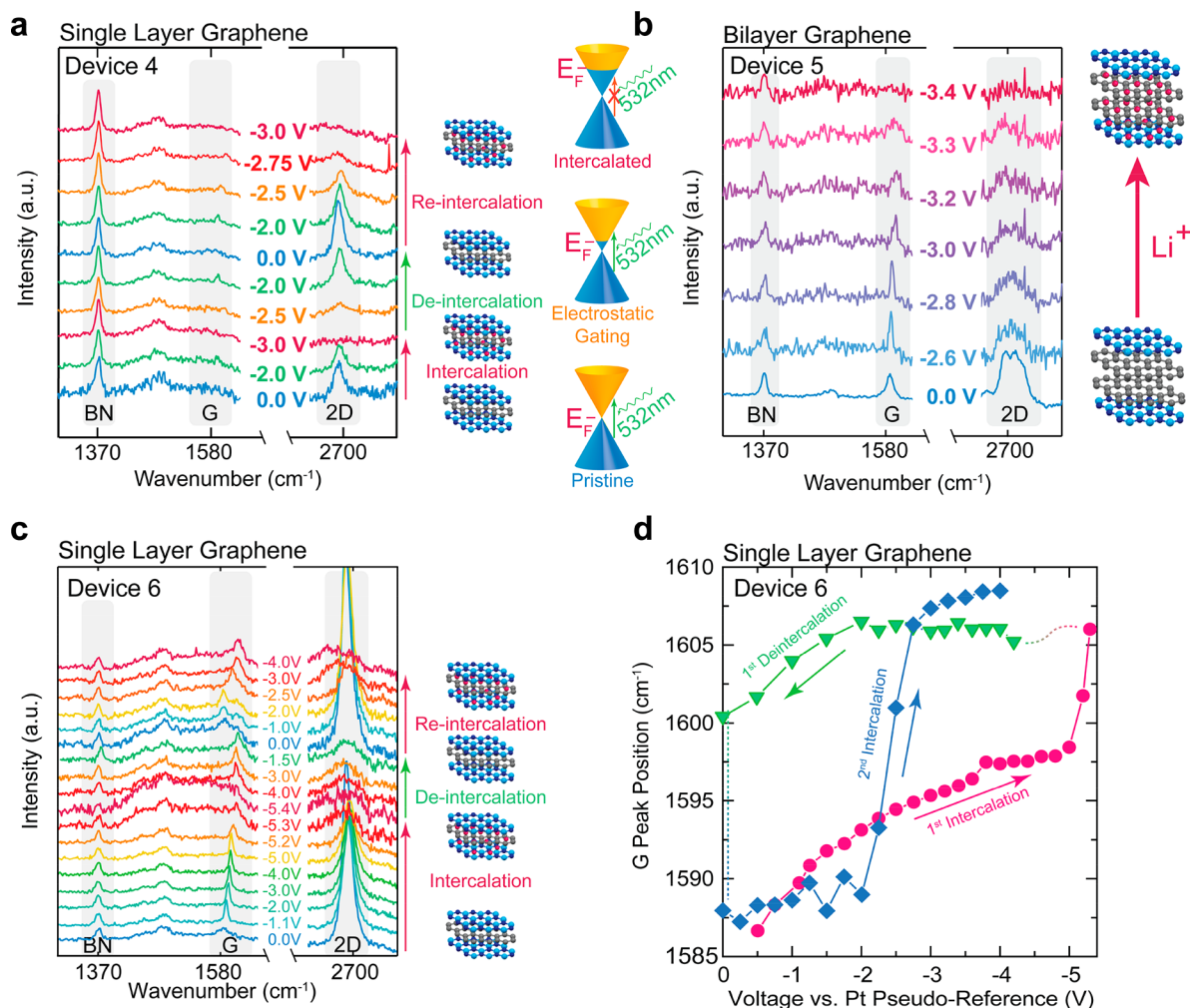
Figure 3. (a−c) Representative Raman spectra demonstrating the evolution of the G and 2D peaks with applied potential while the h-BN peak remains constant for 1LG (a, c) and 2LG (b) encapsulated in h-BN. The electrolyte fluorescence background is subtracted from all Raman spectra, and the spectra are offset for clarity. Note the gradual blue-shift in the graphene G peak. Beyond the threshold intercalation voltage, all graphene spectroscopic signatures disappear. Dirac cones show, schematically, the doping of the graphene crystal and subsequent Pauli blocking. The relative intensities of the peaks differ from optical interference effects[14] arising form differences in the heterostructure thickness, due to the choice of h-BN crystals. (d) G-peak position measured from the spectra shown in part c as a function of applied voltage for 1LG encapsulated in h-BN. Note the sudden change in G peak position, showing that the graphene had suddenly intercalated after reaching the threshold voltage. The threshold voltage in parts c and d was higher than other devices because the contact resistance between gold and graphene was abnormally high in this particular device.

graphene intercalations.[15,16] Specifically, both the G- and 2D-peaks of graphene (near 1582 and 2700 cm^{-1}, respectively, in pristine graphene) are good indicators of the charge density in the graphene basal plane.[16,17]

We performed *in situ* Raman spectroelectrochemistry to further confirm that Li ions can intercalate the graphene/h-BN interface. Figure 3 shows the evolution of the Raman G and 2D peaks of graphene as a function of applied cell potential for both 1LG and 2LG samples. The 1LG structure is once again very instructive. As the cell potential increases, the graphene G peak sharpens and shifts at low voltages due to increasing carrier density in graphene. A fit of the G peak position in Figure 3d suggests that the carrier density increases approximately linearly with the applied voltage (so that the Fermi energy increases approximately as $V_{\mathrm{eg}}^{1/2}$), consistent with electrostatic gating through the h-BN layer. As the cell voltage approaches the threshold, the G peak rapidly blue-shifts, and both G and 2D peaks subsequently disappear, while the corresponding h-BN peak[18] at 1370 cm^{-1} remains visible.

This suggests that the graphene layer is sufficiently doped by the Li intercalant as to be Pauli-blocked, while the h-BN layer remains unaffected. Comparison with graphite literature[16] shows that Pauli-blocking and the vanishing of the graphite Raman peaks is a signature of stage 1 intercalation in bulk Li intercalated graphite LiC$_6$. This observation further suggests that Li is coming into direct contact with the graphene, and supports the notion of graphene/h-BN interface intercalation. Using the excitation laser wavelength ($\lambda = 532$ nm) as a lower bound for the Fermi energy, the graphene was doped to $E_{\mathrm{F}} > 1.16$ eV, corresponding to a charge density of 9.9×10^{13} cm^{-2}, a very high carrier density normally inaccessible using electrostatic gating through a thick h-BN crystal alone.

In both the 1LG and 2LG heterostructures, the Raman spectra do not exhibit an appreciable D peak at 1350 cm^{-1}, which is commonly associated with chemical disorder or damage of the in-plane covalent graphene bonds.[19] The absence of Raman D peak during the intercalation/de-intercalation process suggests that the Li ions are inserted
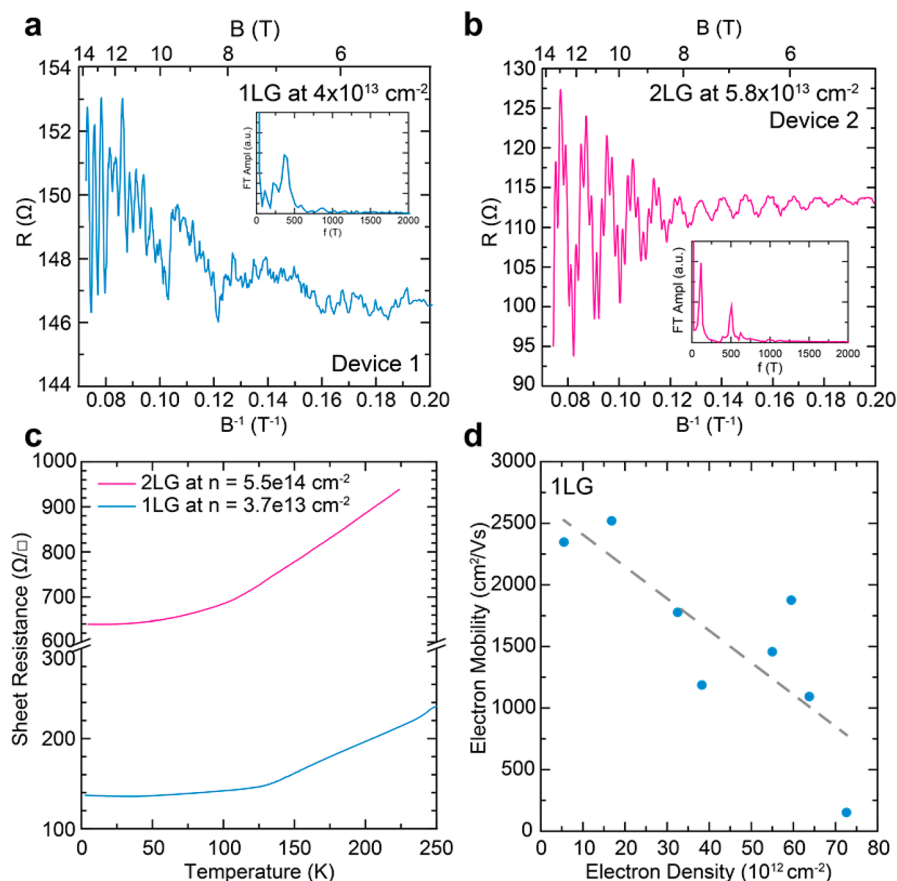
Figure 4. (a) Measured R_{xx} as a function of B^{-1} in a 1LG device with Hall carrier density 4.0×10^{13} cm^{-2} at 1.8 K. Periodic SdH oscillations are visible. The inset shows the Fourier transform of SdH, indicating a peak corresponding to the carrier density $(3.66 \pm 0.08) \times 10^{13}$ cm^{-2}. (b) R_{xx} as a function of B^{-1} in a 2LG device with Hall carrier density 5.8×10^{13} cm^{-2} at 1.8 K. The inset shows the Fourier transform of SdH, indicating two peaks corresponding to the carrier densities $(1.07 \pm 0.01) \times 10^{13}$ and $(4.84 \pm 0.01) \times 10^{13}$ cm^{-2}. (c) Resistivity of intercalated 1LG (blue) and 2LG (red) heterostructures at cryogenic temperatures, showing metallic behavior. (d) Electron mobility vs electron density from multiple intercalated 1LG devices, cooled to below 10 K. The line is a guide to the eye showing a general decrease of mobility after increasing intercalation.

into the graphene/h-BN interface without damaging the in-plane bonds between the carbon atoms, leaving the graphene lattice itself intact. Furthermore, Raman spectra taken on the same device through multiple cycles (Figure 3a,c) demonstrate the reversibility of the Raman behavior. The graphene Raman peaks reappear when we reach a threshold voltage during the reverse cell potential scan. A second intercalation cycle produces similar Raman spectra as the first cycle with the G peak shifting as a function of gate potential.

The 2LG structure undergoes two forms of intercalation: at the graphene/graphene interface and at the graphene/h-BN interface. We observe behavior in Raman that cannot be ascribed solely to intercalation of the graphene/graphene interface (Figure 3b). In bulk graphite, stage 2 behavior (LiC$_{12}$), which denotes that only one side of each graphene layer is occupied by the intercalant, is characterized by a broadened, blue-shifted, but nevertheless present G peak.[16] In our 2LG device, the Raman G and 2D peaks both disappear at high voltage (while the h-BN D mode remains unchanged), indicating doping beyond the C$_6$LiC$_6$ stage (>3 × 10^{14} cm^{-2}) for each layer of graphene.

The cycling Hall measurement described above was performed at slightly elevated temperature (325 K or 52 °C) to enable simultaneous monitoring of the carrier density during the intercalation process. We also performed low temperature transport characterization of intercalated samples. For this

experiment, the intercalated device was cooled quickly (at a cooling rate of ~10 K/min) while holding the applied cell potential. It is known that Li ions become immobile in the PEO matrix when cooled below the polymer glass transition temperature of $T_g \sim 200$ K. Below T_g, all electrochemical processes are completely frozen out and no de-intercalation processes occur even when the cell potential is brought back to 0 V. This allows us to create stable intercalated vdW heterostructures.

With the samples frozen at a predefined electrochemical potential, we measure the Hall voltage as a function of the applied magnetic field. We find that the electron density of the 1LG heterostructures saturates around a maximum of ~7 × 10^{13} cm^{-2}, although the exact value varies between devices and maximum applied electrochemical potentials. On the basis of density functional theory (DFT) calculations suggesting that each intercalating Li ion donates 0.88 electron charge to the conducting graphene system,[10] we calculate a Li:C stoichiometric ratio of approximately 1:60, about $^1/_{10}$ of the electron density of stage 1 Li intercalated bulk graphite. This ratio is smaller yet consistent with our DFT calculations suggesting an upper bound of Li:C stoichiometry ~1:20 in h-BN/graphene/h-BN sandwich structure (see Figure S1 in the Supporting Information). Overall, this data indicates that the graphene/h-BN interface is far less amenable to hosting Li atoms than two neighboring graphene planes.

The intercalation process injects a large number of Li ions into the graphene/h-BN heterostructure. At the Li densities achieved here, the Li atoms are likely to be distributed randomly relative to the graphene lattice, creating scattering sites for the conducting electrons in graphene.[11] Correspondingly, we observe a large decrease in mobility after intercalation, from ~200 000 cm^2/(V s) readily achieved in clean 1LG devices to approximately ~1500 cm^2/(V s). Despite this relatively low mobility value, we observe Shubnikov−de Haas (SdH) oscillation of magnetoresistance R_{xx} as a function of applied magnetic field B at 1.8 K (Figure 4a). The observed SdH oscillations in intercalated 1LG heterostructure exhibit a single period oscillation in B^{-1} (inset in Figure 4a). Assuming spin and valley degeneracy of 1LG, the density estimated from SdH oscillation is 4×10^{13} cm^{-2}, in agreement with the density measured from the Hall measurement.

Similar measurements performed on 2LG heterostructures revealed the maximum carrier density up to 5.5×10^{14} cm^{-2}. By assuming that the carrier density of the graphene/h-BN interfaces in 2LG matches that of the 1LG heterostructure (7×10^{13} cm^{-2}), we can estimate an electron density in the graphene/graphene interface of 4.8×10^{14} cm^{-2}. This data indicates that the graphene−graphene interface can host significantly more Li ions than the h-BN/graphene interface in agreement with our DFT calculation (see the Supporting Information).

SdH oscillations are also visible in the 2LG devices but only if the electron density is kept low ($<6 \times 10^{13}$ cm^{-2}) by keeping the cell potential close to the threshold before the cooldown. As shown in Figure 4b, the SdH oscillations show two distinct frequencies, unlike the 1LG case, corresponding to conduction in two separate bands. Two similar SdH oscillation frequencies have been observed in electrolytically gated bilayer graphene samples,[20] suggesting different populations in the lower and higher subbands of 2LG. In our experiment, the total carrier density in both bands matches with the value derived from Hall data.

Finally, we discuss the temperature dependent transport in the intercalated compound. For this measurement, we slowly warm up the samples (warming up rate ~5 K/min) under magnetic field and measure R_{xx} and Hall resistance R_{xy} of the samples to obtain the density and mobility of the samples at different temperatures. Figure 4c shows that R_{xx} increases monotonically for 1LG and 2LG as temperature increases, indicating metallic behaviors of both samples. We note that both mobility and density typically remain approximately constant below 200 K. However, when the intercalated devices are warmed above the polymer T_g, chemical reactions resume as a function of the cell potential. We note that the electron mobility decreases significantly at higher temperatures and at higher doping. At the highest carrier density of 5.5×10^{14} cm^{-2} for 2LG, the electron mobility decreases to ~18 cm^2/(V s) when $T < 100$ K. An overview of the mobilities attained in multiple 1LG devices intercalated to different densities is presented in Figure 4d. We observe a general trend in decreasing mobility with increasing intercalation density, consistent with increasing intervalley scattering due to increasing numbers of Li ions associated with the graphene layer.

In summary, we have demonstrated the electrochemical intercalation of Li into graphene encapsulated between h-BN layers. Passsivation of the device components (graphene surface and electrodes) prevents electrochemical side reactions that lead to the modification of the sample surface. Our device platform allows for *in situ* characterization of the doping level and electrical transport properties as the intecalation progresses. Using our Hall potentiometry method, we can not only very precisely monitor the intercalation through Hall effect, but we can also intercalate the galleries in the graphene/h-BN interface. The effect of intercalation into vdW heterostructure is most prominent in the 1LG case, where gating effects are not enough to explain the observed high doping levels in both the Raman and transport data. Our technique enables the engineering of novel vdW heterostructures with diverse functionality and applications.

■ ASSOCIATED CONTENT

Ⓢ Supporting Information

The Supporting Information is available free of charge on the ACS Publications website at DOI: 10.1021/acs.nanolett.7b04396.

SI contains our DFT calculation showing the stability of the lithium intercalated graphene/h-BN interface, detailed experimental methods, and measurements on the uniformity of our samples while undergoing intercalation (PDF)

■ AUTHOR INFORMATION

Corresponding Author

*E-mail: pkim@physics.harvard.edu.

ORCID Ⓘ

Dmitri K. Efetov: 0000-0001-5862-0462

Yinsheng Guo: 0000-0002-0571-8447

Louis E. Brus: 0000-0002-5337-5776

Xavier Roy: 0000-0002-8850-0725

Philip Kim: 0000-0002-8255-0086

Present Addresses

D.K.E.: ICFO - The Institute of Photonic Sciences, Mediterranean Technology Park, Av. Carl Friedrich Gauss 3, 08860 Castelldefels (Barcelona), Spain.

Y.G.: Department of Chemistry, Northwestern University, Evanston, Illinois 60208, United States.

J.R.: Mork Family Department of Chemical Engineering and Materials Science, University of Southern California, Los Angeles, California 90089, United States.

Notes

The authors declare no competing financial interest.

■ ACKNOWLEDGMENTS

■ REFERENCES

(1) Dresselhaus, M. S.; Dresselhaus, G. *Adv. Phys.* **1981**, *30* (1), 139−326, DOI: 10.1080/00018738100101367.

(2) Weller, T. E.; Ellerby, M.; Saxena, S. S.; Smith, R. P.; Skipper, N. T. *Nat. Phys.* **2005**, *1* (1), 39.

(3) Cahen, S.; Lagrange, P.; Mareche, J.-F.; Herold, C. *C. R. Chim.* **2013**, *16* (4), 385−390.

(4) Bao, W. Z.; Wan, J. Y.; Han, X. G.; Cai, X. H.; Zhu, H. L.; Kim, D.; Ma, D. K.; Xu, Y. L.; Munday, J. N.; Drew, H. D.; Fuhrer, M. S.; Hu, L. B. *Nat. Commun.* **2014**, *5*, 4224.

(5) Chapman, J.; Su, Y.; Howard, C. A.; Kundys, D.; Grigorenko, A. N.; Guinea, F.; Geim, A. K.; Grigorieva, I. V.; Nair, R. R. *Sci. Rep.* **2016**, *6*, 23254.

(6) Kim, N. D.; Kim, K. S.; Jung, N. Y.; Brus, L.; Kim, P. *Nano Lett.* **2011**, *11*, 860.

(7) Weeks, C.; Hu, J.; Alicea, J.; Franz, M.; Wu, R. Q. *Phys. Rev. X* **2011**, *1*, 021001.

(8) Dean, C. R.; Young, A. F.; Meric, I.; Lee, C.; Wang, L.; Sorgenfrei, S.; Watanabe, K.; Taniguchi, T.; Kim, P.; Shepard, K. L.; Hone, J. *Nat. Nanotechnol.* **2010**, *5*, 722.

(9) Dean, C. R.; Wang, L.; Maher, P.; Forsythe, C.; Ghahari, F.; Gao, Y.; Katoch, J.; Ishigami, M.; Moon, P.; Koshino, M.; Taniguchi, T.; Watanabe, K.; Shepard, K. L.; Hone, J.; Kim, P. *Nature* **2013**, *497*, 598.

(10) Shirodkar, S. N.; Kaxiras, E. *Phys. Rev. B: Condens. Matter Mater. Phys.* **2016**, *93*, 245438.

(11) Kuhne, M.; Paolucci, F.; Popovic, J.; Ostrovsky, P. M.; Maier, J.; Smet, J. H. *Nat. Nanotechnol.* **2017**, *12*, 895−900.

(12) Wang, L.; Meric, I.; Huang, P. Y.; Gao, Q.; Gao, Y.; Tran, H.; Taniguchi, T.; Watanabe, K.; Campos, L. M.; Muller, D. A.; Guo, J.; Kim, P.; Hone, J.; Shepard, K. L.; Dean, C. R. *Science* **2013**, *342*, 614.

(13) Efetov, D. K.; Kim, P. *Phys. Rev. Lett.* **2010**, *105*, 256805.

(14) Yoon, D.; Moon, H.; Son, Y. W.; Choi, J. S.; Park, B. H.; Cha, Y. H.; Kim, Y. D.; Cheong, H. *Phys. Rev. B: Condens. Matter Mater. Phys.* **2009**, *80*, 125422.

(15) Jung, N. Y.; Kim, N. D.; Jockusch, S.; Turro, N. J.; Kim, P.; Brus, L. *Nano Lett.* **2009**, *9* (12), 4133−4137.

(16) Inaba, M.; Yoshida, H.; Ogumi, Z.; Abe, T.; Mizutani, Y.; Asano, M. *J. Electrochem. Soc.* **1995**, *142* (1), 20.

(17) Chen, C.-F.; Park, C.-H.; Boudouris, B. W.; Horng, J.; Geng, B.; Girit, C.; Zettl, A.; Crommie, M. F.; Segalman, R. A.; Louie, S. G.; Wang, F. *Nature* **2011**, *471*, 617−620.

(18) Geick, R.; Perry, C. H.; Rupprecht, G. *Phys. Rev.* **1966**, *146* (2), 543.

(19) Ferrari, A. C.; Meyer, J. C.; Scardaci, V.; Casiraghi, C.; Lanzzeri, M.; Mauri, F.; piscanec, S.; Jiang, D.; Novoselov, K. S.; Roth, S.; Geim, A. K. *Phys. Rev. Lett.* **2006**, *97*, 187401.

(20) Efetov, D. K.; Maher, P.; Glinskis, S.; Kim, P. *Phys. Rev. B: Condens. Matter Mater. Phys.* **2011**, *84*, 161412.